Discovery of BUB1 kinase inhibitors for the treatment of cancer

Bosman, R.E.J.

7

Summary and future prospects

Cancer is the overarching term for diseases in which abnormal cells divide in an uncontrolled manner.[1] These cells can develop in and may subsequently spread to different types of tissue. Hallmarks of cancer, which are biological capabilities that are acquired during the development of a tumor, include, but are not limited to, sustaining proliferative signaling, resisting cell death and metastasis.[2] In addition, there are characteristics that enable their acquisition, including genetic instability.[2] The development of new anti-cancer drugs can therefore be aimed at one or multiple hallmarks or at characteristics that enable these hallmarks.[2] The research described in thesis covers several phases of a drug discovery program (**Figure 7.1**) aimed at the discovery of small molecule kinase inhibitors for the treatment of cancer. This chapter summarizes the work described in previous chapters and provides future directions for further optimization and applications of the inhibitors.

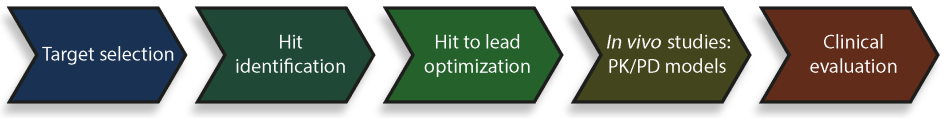

Figure 7.1 | Simplified scheme of the different phases in drug discovery.

Target selection

Protein kinases are a prominent class of drug targets for the treatment of cancer.[3] **Chapter 1** introduces the protein kinase budding uninhibited by benzimidazole 1 (BUB1) as therapeutic target. BUB1 participates in the spindle assembly checkpoint (SAC), which is a safety mechanism during mitosis that ensures correct chromosome segregation.[4] Many cancer cells suffer from a weakened SAC and interference with these diminished checkpoints to further disrupt SAC signaling is hypothesized to eventually result in cell death due to severe chromosomal instability.[5,6] Potential kinase targets of the SAC include monopolar spindle 1 (MPS1) and BUB1.[5,6] Previously, MPS1 inhibitors have been developed, some of which have entered clinical trials.[7–9] However, multiple mouse xenograft studies on MPS1 inhibitors only showed single agent efficacy when administered near the maximum tolerated dose and cotreatment with taxanes was therefore necessary to obtain the desired inhibition of tumor growth.[10–13] Novel inhibitors with good physicochemical properties that allow cellular BUB1 target engagement may result in single agent efficacy. This would make cotreatment with taxanes dispensable, which is desired in view of the fact that these agents cause severe side effects.[14] BUB1 was therefore selected as target for the discovery of novel inhibitors.

Hit identification

Chapter 2 describes the results of a high-throughput screen which was used for the discovery of novel BUB1 inhibitors. A library of 53,408 compounds, enriched with kinase inhibitors, was screened and resulted in 214 confirmed actives. After deselecting compounds that interfered with the assay readout, and dose-response experiments, a qualified hit list of 25 structurally diverse molecules was obtained. Hits **1** and **2** (**Figure 7.2**) were prioritized based on their

favorable properties such as activity, molecular weight, ligand efficiency, lipophilicity and lipophilic efficiency.[15] Both hits were resynthesized and their activities were confirmed.

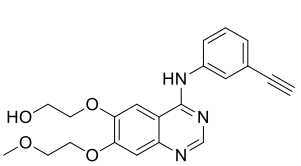

1

pIC_{50} = 6.59
MW = 379
LE = 0.33
cLogP = 2.6
LipE = 4.2

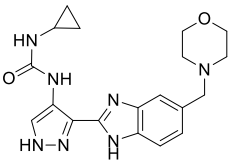

2

pIC_{50} = 6.78
MW = 381
LE = 0.34
cLogP = 0.4
LipE = 6.5

Figure 7.2 | Prioritized hits **1** and **2** of high-throughput screen and corresponding physicochemical properties. pIC_{50}: half maximal inhibitory concentrations from high-throughput dose-response assay; MW: molecular weight (g/mol); LE: ligand efficiency[15], defined as: $\mathrm{LE} = (-RT * \ln(\mathrm{app}.K_i))/\mathrm{HA}$, where HA stands for the number of 'heavy atoms' (non-hydrogen atoms); cLogP: LogP calculated by DataWarrior (v.5.2.1); LipE: lipophilic efficiency[15], defined as: $\mathrm{LipE} = \mathrm{app}.\mathrm{p}K_i - \mathrm{cLogP}$.

Hit to lead optimization

In **Chapter 3**, the structure-activity relationship (SAR) of hit **1** was investigated. Synthesis and biochemical evaluation of 48 analogues resulted in the identification of compound **3** (**Figure 7.3**). Compared to hit **1**, compound **3** which was significantly less lipophilic and due to its slightly improved potency, a 10-fold better lipophilic efficiency was obtained. The docking pose of compounds **1** and **3** in the kinase domain of BUB1 matched with the observed SAR. Whereas the quinazoline *N*1 of **1** formed a hydrogen bond with the backbone of hinge amino acid Tyr869, no hydrogen bonds were established with the hinge region in the docking pose of compound **3**. Instead, hydrogen bond formation was predicted between the pyrazole *N*2 and both Lys821 and Asp946 as well as between the pyrimidine *N*1 and Lys821.

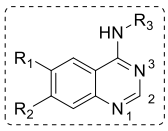

General structure

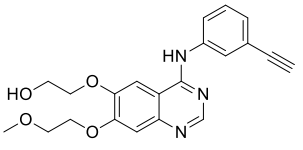

1

pIC_{50} = 6.28 ± 0.05
app.K_i = 185 nM
MW = 379
cLogP = 2.6
LipE = 4.1
tPSA = 85

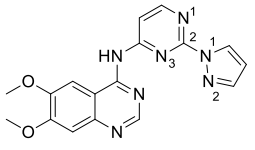

3

pIC_{50} = 6.41± 0.04
app.K_i = 136 nM
MW = 349
cLogP = 1.7
LipE = 5.1
tPSA = 96

Figure 7.3 | Chemical structures and physicochemical properties (as defined in **Figure 7.2**) of hit **1** and optimized hit **3**. pIC_{50}: half maximal inhibitory concentration, determined by the biochemical BUB1 assay; tPSA: topological polar surface area (Å^2), calculated by Chemdraw (v.19.1).

Chapter 4 describes a comprehensive structure-activity relationship (SAR) study of hit **2**. In total, 59 analogues were synthesized and biochemically evaluated. This yielded substituted 2-phenyl-5-methoxy-*N*-(3-(5-(morpholinomethyl)-1*H*-benzo[*d*]imidazol-2-yl)-1*H*-pyrazol-4-yl)pyrimidin-4-amines as highly potent BUB1 inhibitors, including compound **4** (**Figure 7.4A**), which is the most potent BUB1 inhibitor reported to date. To study the binding mode of **4**, the crystal structure of this compound bound to the kinase domain of BUB1 was elucidated (**Figure 7.4B,C**). Compound **4** binds in the ATP pocket of BUB1 leaving the regulatory (R)-spine[16] intact. This indicated that **4** can be classified as a type I inhibitor.[17] The benzimidazole-pyrazole scaffold forms three hydrogen bonds with the backbone of hinge amino acids Tyr869 and Glu867 of BUB1 (**Figure 7.4B**). An additional hydrogen bond is formed between the pyrimidine *N*1 and the side chain of Lys821 which is mediated by a water molecule. Furthermore, the morpholine is solvent exposed and the amine between the pyrazole and pyrimidine forms an intramolecular hydrogen bond with the benzimidazole nitrogen. The acetylene binds a pocket that is available due to the small size of the glycine gatekeeper residue of BUB1 (**Figure 7.4C**).

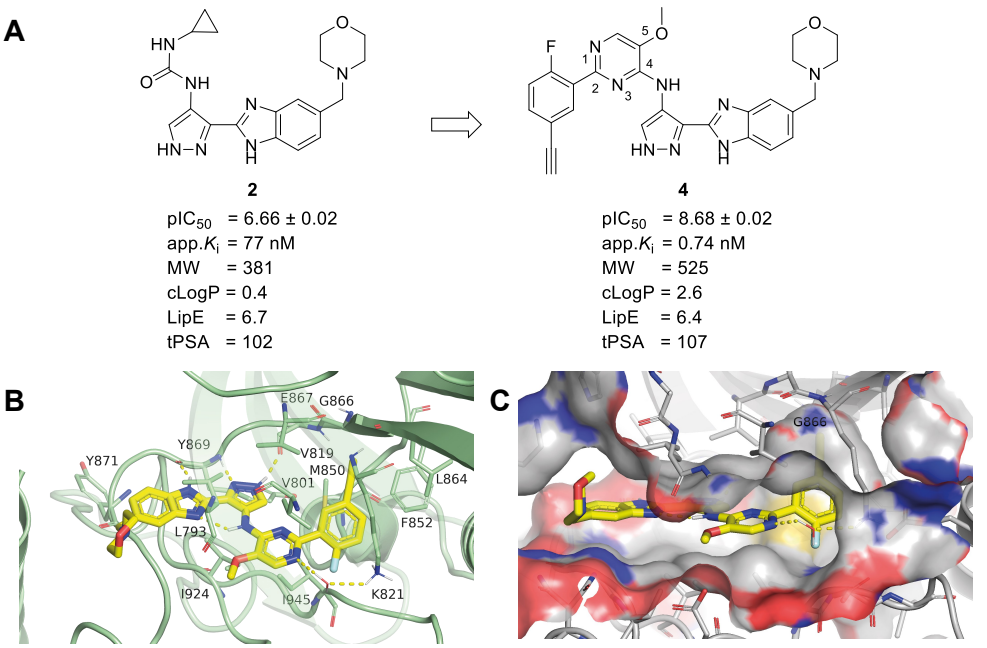

Figure 7.4 | Hit optimization and crystal structure of optimized compound 4 bound to the kinase domain of human BUB1. (A) Chemical structures and physicochemical properties (as defined in **Figure 7.3**) of hit **2** and optimized compound **4**. **(B)** Crystal structure of **4** bound to BUB1. Hydrogen bonds are visualized by dashed lines (yellow) and a water molecule is represented by small sticks. β-sheets 1–3 are semi-transparent for visualization purposes. **(C)** Representation of the surface around amino acids within 8 Å from **4**.

Chapter 5 describes the development of a cellular BUB1 target engagement assay using probe **5**[18] (**Figure 7.5**) and gel-based activity-based protein profiling (ABPP). Probe **5** as well as 16 analogues were synthesized. To study BUB1 labeling, a U2OS cell line was generated that stably overexpressed GFP-FLAG-BUB1. Labeling by all probes was evaluated in this cell

line and probe **5** was found to show the most favorable labeling profile. Mutating Cys1080 to alanine completely abolished BUB1 labeling indicating that this amino acid is responsible for the formation of a covalent bond. Labeling of BUB1 by probe **5** was dose- and time-dependent and labeling could dose-dependently be outcompeted by BUB1 inhibitor BAY1816032.[19] This provided proof-of-principle for the use of **5** as BUB1 chemical probe that allows for studying cellular BUB1 target engagement using gel-based ABPP.

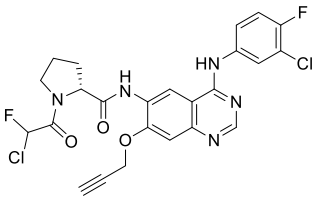

5

Figure 7.5 | Chemical structure of probe **5**.[18]

Chapter 6 focuses on further profiling a subset of the substituted 2-phenyl-5-methoxy-*N*-(3-(5-(morpholinomethyl)-1*H*-benzo[*d*]imidazol-2-yl)-1*H*-pyrazol-4-yl)pyrimidin-4-amine BUB1 inhibitors identified in **Chapter 4** to study their potential as lead candidates for therapeutic purposes. To this end, drug-likeness was studied by investigation of several *in vitro* absorption, distribution, metabolism and excretion (ADME) assays. In addition, cellular BUB1 target engagement was investigated by using the assay developed in **Chapter 5**. A strong correlation was found between biochemical pIC_{50} values and BUB1 target engagement (Pearson's r: 0.921, *p*-value: 0.0004), which suggested that cell permeability was similar among the compounds tested and that target engagement was mainly driven by the affinity for BUB1. Furthermore, the effects on U2OS cell proliferation were explored by sulforhodamine B (SRB) assays. These assays were performed with and without a low dose of paclitaxel to investigate potential synergistic effects between BUB1 inhibition and paclitaxel.[19] A moderate correlation was found between BUB1 target engagement and pIC_{50} values of the SRB assays (Pearson's r: 0.655, *p*-value: 0.056). This suggested that inhibition of cell proliferation was, to a large extent, dependent on BUB1 inhibition, but that off-target activity contributed to the observed effect. ROB433 (**6**) and ROB464 (**7**) showed the most favorable profile (**Figure 7.6**, **Table 7.1**) with good physicochemical properties, subnanomolar affinity for BUB1, good cellular BUB1 target engagement and an acceptable *in vitro* ADME profile. Therefore, kinase selectivity was assessed for these compounds. At 100 nM, ROB433 and ROB464 were selective over 346 and 352 kinases, respectively, while 49 (ROB433) and 44 (ROB464) kinases were detected as off-targets. Finally, the antiproliferative activity of ROB433 (**6**) was assessed in a panel of 102 cancer cell lines. Concentrations required for half maximal growth inhibition (GI_{50}) ranged from 101 nM (for KG-1 cells) to 5.57 µM (for THP-1 cells). The mean GI_{50} value among all cell lines was 1.43 µM, which indicated that ROB433 has a favorable cytotoxicity profile.

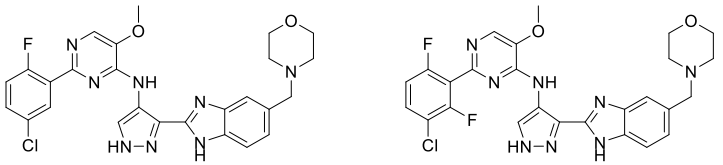

ROB433 (**6**) ROB464 (**7**)

Figure 7.6 | Chemical structures of ROB433 (**6**) and ROB464 (**7**).

Table 7.1 | Summary of physicochemical properties (as defined in **Figure 7.3**), ADME properties, aqueous solubility and activities of lead compounds ROB433 (**6**) and ROB464 (**7**).

	ROB433	**ROB464**		**ROB433**	**ROB464**
Biochemical activity (pIC_{50} ± SEM)	8.57 ± 0.02	8.62 ± 0.03	**Target engagement** (pTE_{50} ± SEM)	7.50 ± 0.11	8.01 ± 0.09
Apparent K_i (nM)	0.94	0.84	**U2OS cell proliferation** (pIC_{50} ± SEM)	6.32 ± 0.06	7.39 ± 0.05
Molecular weight (g/mol)	535	553	**Plasma stability** (% remaining after 180 min)	100 (h)* 100 (r)* 85 (m)*	100 (h) 100 (r)
cLogP	3.1	3.2	**Microsomal stability** ($t_{1/2}$ in min)	41 (h) 63 (r) 22 (m)	29 (h) 49 (r) 6.1 (m)
LipE	5.9	5.8	**Microsomal clearance** (µL/min/mg)	8.4 (h) 22 (r) 16 (m)	12 (h) 28 (r) 57 (m)
tPSA ($Å^2$)	107	107	**Plasma protein binding** (%)	100 (h) 100 (r) 99.9 (m)	99.7 (h) 99.7 (r)
			Aqueous solubility (µM)	4.4	6.0

* (h): human, (r): rat, (m): mouse

Future directions

Chapter 3 describes the optimization of hit **1** to compound **3**. Docking studies revealed a different binding mode of **3** when compared to that of hit **1**, in which the quinazoline *N1* did not form a hydrogen bond with the hinge region of BUB1. To provide evidence for this proposed binding mode, a compound lacking the quinazoline *N*1 is proposed (**Figure 7.7**). If this molecule would show similar activity, it may indeed suggest that it does not interact with the hinge region of BUB1 and its predicted binding mode may provide future directions for further analogue design.

The use of covalent drugs is an alternative approach to reversible kinase inhibition and has been shown to have several benefits.[20] Due to the formation of a covalent bond, irreversible inhibitors have high potencies due to prolonged target occupancy. In addition, when off-target binding only occurs in a reversible fashion, better selectivity can be achieved. Furthermore, covalent inhibitors might be less prone to acquired resistance, as was reported for covalent EGFR inhibition, which upon the T790M mutation improved affinity for ATP and

thereby reduced efficacy of reversible inhibitors.[21,22] **Chapter 5** describes the validation of compound **5** (**Figure 7.5**) as BUB1 probe which was found to covalently react with BUB1. Compound **5** therefore provides an excellent starting point for the development of irreversible BUB1 inhibitors. However, optimization of **5** proved challenging. Therefore, crystallization of this compound in the kinase domain of BUB1 would allow for a more rational design of novel covalent BUB1 inhibitors.

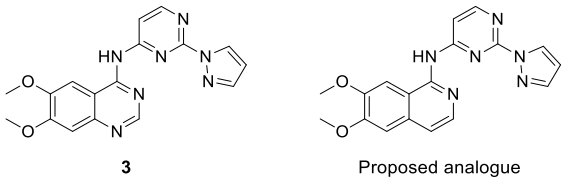

Figure 7.7 | Proposed analogue of **3** to provide evidence for its predicted binding mode.

BUB1 is known to phosphorylate histone H2A at threonine 120.[23] The importance of the enzymatic activity of BUB1 in chromosome alignment is less well established since contradicting results have been published.[24–27] In **Chapter 6**, ROB433 (**6**) and ROB464 (**7**) were identified as lead BUB1 inhibitors with good cellular BUB1 target engagement which provide opportunities to study aforementioned processes. A preliminary (N=1) study on the effects of BUB1 inhibition on H2A phosphorylation and chromosome alignment was therefore performed. To this end, human retinal pigment epithelial 1 (RPE1) cells, which are frequently used to study mitosis[28], were synchronized in the G_2 phase by CDK1 inhibitor RO-3306.[29] After drug washout, cells were treated with monastrol, which causes monopolar spindles due to inhibition of motor protein kinesin Eg5.[30] Simultaneously, cells were treated with a BUB1 inhibitor. Subsequently, another drug washout was performed to allow for bipolar spindle assembly. Cells were then treated with MG132, a proteasome inhibitor to prevent mitotic exit[31], and a BUB1 inhibitor. H2A phosphorylation was visualized by immunofluorescence staining using an anti-H2A-p-T120 antibody. In addition, chromosome alignment was investigated by staining of CENP-C, located at the inner kinetochore, tubulin and DNA.

Quantification of H2A phosphorylation (H2A-p-T120) revealed a significant reduction of H2A-p-T120 signal upon treatment with 100 nM of ROB433 and ROB464 (**Figure 7.8A,C**). This confirmed inhibition of BUB1 in a cellular system. In contrast, 300 nM of BAY1816032 was required to match these results. To study chromosomal alignment, the immunofluorescence images were used to classify cells into different phenotypes based on their extent of chromosome alignment as determined by DAPI staining of DNA. Chromosome alignment was dose-dependently impaired and more profound for ROB464 compared to ROB433 (**Figure 7.8B,C**). BAY1816032 only moderately increased chromosome alignment errors at both concentrations. Based on the observation that 100 nM ROB433 and ROB464 inhibited Aurora B *in vitro* (71 and 43%, respectively, **Chapter 6**), Aurora B may also be (partially) inhibited in living cells. To investigate this, phosphorylation of one of Aurora B's

targets, histone H3 at Ser10[32], was investigated as described above. Immunofluorescence staining by an anti-H3-p-S10 antibody revealed a significant reduction in phosphorylation of H3Ser10 (H3-p-S10) in both ROB433 and ROB464 treated cells (**Figure 7.9A,C**). This reduction was similar to cells treated with Aurora B inhibitor ZM447439[33] (2 µM). Interestingly, BAY1816032 also reduced phosphorylation of H3Ser10, whereas no *in vitro* inhibition of Aurora B was observed for this compound.[19] Previously, BUB1-mediated H2A phosphorylation has been reported to control the localization and activity of Aurora B.[27] Whether direct inhibition of Aurora B by ROB433 and ROB464 is responsible for the observed reduction of histone H3-S10 phosphorylation or that this is mediated via a reduction of H2A-T120 phosphorylation, remains to be investigated. Of note, the fractions of moderately and heavily misaligned phenotypes for ZM447439 treated cells were similar to those of ROB433 (300 nM) and ROB464 (100 nM) treated cells (**Figure 7.9B,C**).

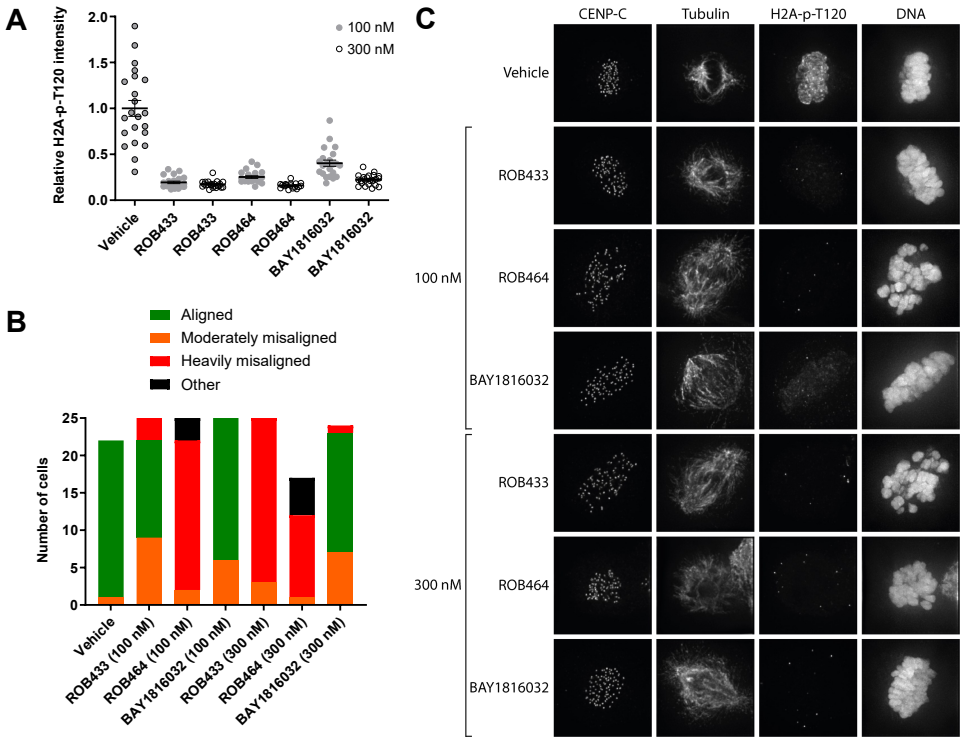

Figure 7.8 | ROB433 and ROB464 reduce phosphorylation of histone H2A-T120 and induce chromosome alignment errors in RPE1 cells. (A) Cells were synchronized by treatment with RO-3306 (5 µM, 16 h), monopolar spindles were induced by treatment with monastrol (200 µM, 2 h), bipolar spindle assembly was then allowed during treatment with MG132 (5 µM, 30 min). Drug washout was performed in between each treatment and during the treatment of monastrol and MG132 cells were cotreated with indicated inhibitor at indicated concentration. Cells were then permeabilized, fixed and immunostained with antibodies for H2A-p-T120, CENP-C and tubulin. DNA was stained by DAPI. The fluorescence intensity of H2A-p-T120 was determined in 22 cells per condition, unless fewer cells were available due to treatment-related cellular defects, and normalized to vehicle-treated cells. **(B)** Cells were treated as in (A) and classified into four different phenotypes based on chromosome alignment as determined by DNA staining: aligned, moderately misaligned, heavily misaligned or other. Phenotypes of 20-25 cells were assessed per condition, unless fewer cells were available due to treatment-related cellular defects. **(C)** Representative images corresponding to graphs in (A) and (B) based on the most predominant phenotype as assessed in (B). Data represent mean with SEM (N=1).

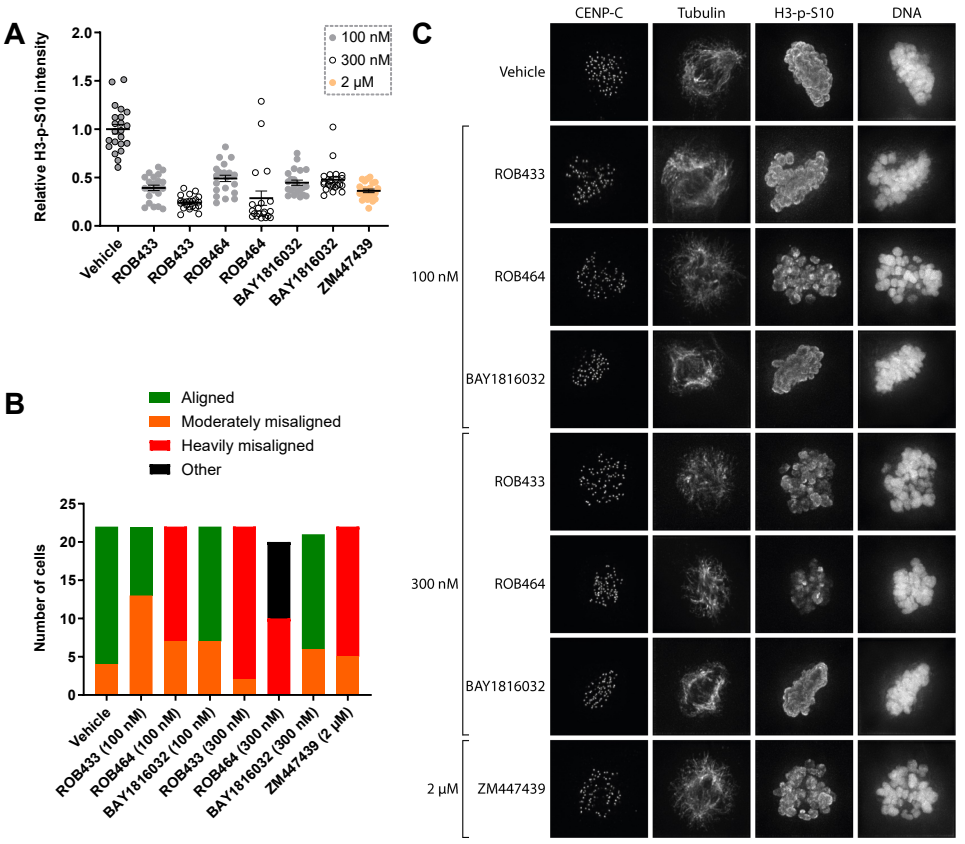

Figure 7.9 | ROB433 and ROB464 reduce phosphorylation of histone H3-S10 and induce chromosome alignment errors in RPE1 cells. (A) Cells were synchronized by treatment with RO-3306 (5 µM, 16 h), monopolar spindles were induced by treatment with monastrol (200 µM, 2 h), bipolar spindle assembly was then allowed during treatment with MG132 (5 µM, 30 min). Drug washout was performed in between each treatment and during the treatment of monastrol and MG132 cells were cotreated with indicated inhibitor at indicated concentration. Cells were then permeabilized, fixed and immunostained with antibodies for H3-p-S10, CENP-C and tubulin. DNA was stained by DAPI. The fluorescence intensity of H3-p-S10 was determined in 22 cells per condition and normalized to vehicle-treated cells. **(B)** Cells were treated as in (A) and classified into four different phenotypes based on chromosome alignment as determined by DNA staining: aligned, moderately misaligned, heavily misaligned or other. Phenotypes of 20-22 cells were assessed per condition. **(C)** Representative images corresponding to graphs in (A) and (B) based on the most predominant phenotype as assessed in (B). Data represent mean with SEM (N=1).

To further provide evidence that the observed phenotypes are attributed to BUB1 inhibition, the cellular selectivity profiles of these compounds need to be investigated. Previously, a broad-spectrum kinase probe, XO44, was published which allowed for capturing over 130 kinases from a single cell line.[34] Such probes can be used for activity-based protein profiling in a chemical proteomics setting to investigate cellular selectivity.[35]

Finally, to assess whether ROB433 and/or ROB464 are suitable for the investigation of their anti-cancer properties, measuring pharmacokinetics is required. Measuring clearance, volume of distribution, half-life, bioavailability and plasma exposure in mice will determine

whether follow-up studies can be performed in mouse xenograft models or that further optimization of these BUB1 inhibitors is required.

Concluding remarks

Research aimed at the identification of novel targets for the treatment of cancer is expanding and small molecule inhibitors fulfill an important role in this process. The research described in this thesis provides two lead inhibitors (ROB433 and ROB464) of the spindle assembly checkpoint kinase BUB1, and an assay to measure cellular BUB1 target engagement. Assessment of cellular BUB1 target occupancy, using the assay described in **Chapter 5**, will be a valuable tool for future development of BUB1 inhibitors. In addition, the series of substituted 2-phenyl-5-methoxy-*N*-(3-(5-(morpholinomethyl)-1*H*-benzo[*d*]imidazol-2-yl)-1*H*-pyrazol-4-yl)pyrimidin-4-amines described in **Chapter 4** include the most active BUB1 inhibitors known to date. Among this series, ROB433 and ROB464 showed excellent properties, including single agent inhibition of cancer cell proliferation, which allow for further evaluation of pharmacokinetic and pharmacodynamic studies *in vivo*. Both compounds hold promise for their therapeutic application in the treatment of cancers which currently lack a molecular target, such as triple-negative breast cancer.

Acknowledgements

From the Hubrecht institute, Maaike Lambers and Carlos Sacristan are kindly acknowledged for performing the immunofluorescence and chromosome alignment assays and Geert Kops for supervision.

Experimental

Cell culture

RPE1 Flp-in cells were cultured at 37°C under 5% CO_2 in Dulbecco's Modified Eagle's Medium/Nutrient Mixture F-12 Ham (DMEM/F12; Sigma D8062) supplemented with 9% (v/v) tetracycline-free fetal bovine serum (FBS), penicillin and streptomycin (50 µg/mL each; Sigma (P0781)).

Immunofluorescence staining

For chromosome alignment assays and measuring histone phosphorylation, RPE1 cells were seeded at 40% confluency in 24-well plates on 1.5H 12 mm coverslips. Cells were synchronized by treatment with RO-3306 (5 µM; Tocris (4181)) for 16 h, washed with pre-warmed DMEM/F12 five times and incubated for 2 h in DMEM/F12 with monastrol (200 µM, Tocris (1305)) and vehicle or inhibitor (indicated concentration) (final concentration (f.c.) DMSO was 0.5%). Cells were then carefully washed four times with pre-warmed DMEM/F12 and incubated for 30 min in DMEM/F12 with MG132 (5 µM, Sigma (C2211)) and vehicle or inhibitor (indicated concentration) (f.c. DMSO was 0.5%), to allow chromosome alignment. Subsequently, cells were permeabilized for 1 min with pre-warmed 0.5% Triton X-100/PHEM buffer (=PIPES (60 mM), HEPES (25 mM), $MgCl_2{\cdot}6H_2O$ (2 mM), EGTA (10 mM), pH 6.9), followed by fixation for 10 min with pre-warmed 4% paraformaldehyde/PBS. After fixation, coverslips were washed three times with PBS and blocked with 3% BSA in PBS for 1 h at RT. Primary antibodies, diluted in 3% BSA in PBS, were added to the coverslips and incubated in a dark, humidified chamber for 16 h at 4°C. Subsequently, cells were washed three times with 0.1% Triton X-100/PBS and incubated with DAPI and secondary antibodies in 3% BSA in PBS for 1 h at RT. Coverslips were washed three times with PBS and mounted onto glass slides using Prolong Gold antifade. All images were acquired on a deconvolution system (DeltaVision Elite Applied Precision/GE Healthcare) with a x100/1.40 NA UPlanSApo objective (Olympus) using SoftWorx 6.0 software (Applied Precision/GE Healthcare). Images were acquired as z-stacks at 0.2-µm intervals and deconvolved using SoftWoRx. Images were quantified using Fiji.[36] Fluorescence intensities were corrected for background signal and normalized to the average intensity of vehicle-treated cells.

Antibodies: guinea pig anti-CENP-C (1:2000, MBL PD030), mouse anti-tubulin (1:10,000, Sigma T5168), rabbit anti-H2A-p-T120 (1:1000, Active motif 39391), rabbit anti-H3-p-S10 (Millipore 06-570), Alexa Fluor 647 goat anti-guinea pig (1:1000, Invitrogen A21450), Alexa Fluor 568 goat anti-mouse (1:1000, Invitrogen A11031), Alexa Fluor 488 goat anti-rabbit (1:1000, Invitrogen A11034) or DAPI (1:1000, Sigma D9542).

References

1. NCI Dictionary of Cancer Terms. *(accessed in September 2021)* https://www.cancer.gov/publications/dictionaries/cancer-terms/def/cancer.
2. Hanahan, D. & Weinberg, R. A. Hallmarks of Cancer: The Next Generation. *Cell* **144**, 646–674 (2011).
3. Cohen, P., Cross, D. & Jänne, P. A. Kinase drug discovery 20 years after imatinib: progress and future directions. *Nat. Rev. Drug Discov.* **20**, 551–569 (2021).
4. Musacchio, A. & Salmon, E. D. The spindle-assembly checkpoint in space and time. *Nat. Rev. Mol. Cell Biol.* **8**, 379–393 (2007).
5. Dominguez-Brauer, C., Thu, K. L., Mason, J. M., Blaser, H., Bray, M. R. & Mak, T. W. Targeting Mitosis in Cancer: Emerging Strategies. *Mol. Cell* **60**, 524–536 (2015).
6. Kops, G. J. P. L., Weaver, B. A. A. & Cleveland, D. W. On the road to cancer: aneuploidy and the mitotic checkpoint. *Nat. Rev. Cancer* **5**, 773–785 (2005).
7. Mason, J. M., Wei, X., Fletcher, G. C., Kiarash, R., Brokx, R., Hodgson, R., Beletskaya, I., Bray, M. R. & Mak, T. W. Functional characterization of CFI-402257, a potent and selective Mps1/TTK kinase inhibitor, for the treatment of cancer. *Proc. Natl. Acad. Sci.* **114**, 3127–3132 (2017).
8. Wengner, A. M., Siemeister, G., Koppitz, M., Schulze, V., Kosemund, D., Klar, U., Stoeckigt, D., Neuhaus, R., Lienau, P., Bader, B., Prechtl, S., Raschke, M., Frisk, A.-L., von Ahsen, O., Michels, M., Kreft, B., von Nussbaum, F., Brands, M., Mumberg, D. & Ziegelbauer, K. Novel Mps1 Kinase Inhibitors with Potent Antitumor Activity. *Mol. Cancer Ther.* **15**, 583–592 (2016).
9. Anderhub, S. J., Mak, G. W.-Y., Gurden, M. D., Faisal, A., Drosopoulos, K., Walsh, K., Woodward, H. L., Innocenti, P., Westwood, I. M., Naud, S., Hayes, A., Theofani, E., Filosto, S., Saville, H., Burke, R., van Montfort, R. L. M., Raynaud, F. I., Blagg, J., Hoelder, S., Eccles, S. A. & Linardopoulos, S. High Proliferation Rate and a Compromised Spindle Assembly Checkpoint Confers Sensitivity to the MPS1 Inhibitor BOS172722 in Triple-Negative Breast Cancers. *Mol. Cancer Ther.* **18**, 1696–1707 (2019).
10. Kusakabe, K., Ide, N., Daigo, Y., Itoh, T., Yamamoto, T., Hashizume, H., Nozu, K., Yoshida, H., Tadano, G., Tagashira, S., Higashino, K., Okano, Y., Sato, Y., Inoue, M., Iguchi, M., Kanazawa, T., Ishioka, Y., Dohi, K., Kido, Y., Sakamoto, S., Ando, S., Maeda, M., Higaki, M., Baba, Y. & Nakamura, Y. Discovery of Imidazo[1,2- *b*]pyridazine Derivatives: Selective and Orally Available Mps1 (TTK) Kinase Inhibitors Exhibiting Remarkable Antiproliferative Activity. *J. Med. Chem.* **58**, 1760–1775 (2015).
11. Martinez, R., Blasina, A., Hallin, J. F., Hu, W., Rymer, I., Fan, J., Hoffman, R. L., Murphy, S., Marx, M., Yanochko, G., Trajkovic, D., Dinh, D., Timofeevski, S., Zhu, Z., Sun, P., Lappin, P. B. & Murray, B. W. Mitotic Checkpoint Kinase Mps1 Has a Role in Normal Physiology which Impacts Clinical Utility. *PLOS ONE* **10**, e0138616 (2015).
12. Maia, A. R. R., de Man, J., Boon, U., Janssen, A., Song, J.-Y., Omerzu, M., Sterrenburg, J. G., Prinsen, M. B. W., Willemsen-Seegers, N., de Roos, J. A. D. M., van Doornmalen, A. M., Uitdehaag, J. C. M., Kops, G. J. P. L., Jonkers, J., Buijsman, R. C., Zaman, G. J. R. & Medema, R. H. Inhibition of the spindle assembly checkpoint kinase TTK enhances the efficacy of docetaxel in a triple-negative breast cancer model. *Ann. Oncol.* **26**, 2180–2192 (2015).
13. Schulze, V. K., Klar, U., Kosemund, D., Wengner, A. M., Siemeister, G., Stöckigt, D., Neuhaus, R., Lienau, P., Bader, B., Prechtl, S., Holton, S. J., Briem, H., Marquardt, T., Schirok, H., Jautelat, R., Bohlmann, R., Nguyen, D., Fernández-Montalván, A. E., Bömer, U., Eberspaecher, U., Brüning, M., Döhr, O., Raschke, M., Kreft, B., Mumberg, D., Ziegelbauer, K., Brands, M., von Nussbaum, F. & Koppitz, M. Treating Cancer by Spindle Assembly Checkpoint Abrogation: Discovery of Two Clinical Candidates, BAY 1161909 and BAY 1217389, Targeting MPS1 Kinase. *J. Med. Chem.* **63**, 8025–8042 (2020).
14. Markman, M. Managing taxane toxicities. *Support. Care Cancer* **11**, 144–147 (2003).
15. Hopkins, A. L., Keserü, G. M., Leeson, P. D., Rees, D. C. & Reynolds, C. H. The role of ligand efficiency metrics in drug discovery. *Nat. Rev. Drug Discov.* **13**, 105–121 (2014).
16. Taylor, S. S. & Kornev, A. P. Protein kinases: evolution of dynamic regulatory proteins. *Trends Biochem. Sci.* **36**, 65–77 (2011).
17. Roskoski, R. Classification of small molecule protein kinase inhibitors based upon the structures of their drug-enzyme complexes. *Pharmacol. Res.* **103**, 26–48 (2016).
18. Shindo, N., Fuchida, H., Sato, M., Watari, K., Shibata, T., Kuwata, K., Miura, C., Okamoto, K., Hatsuyama, Y., Tokunaga, K., Sakamoto, S., Morimoto, S., Abe, Y., Shiroishi, M., Caaveiro, J. M. M., Ueda, T., Tamura, T., Matsunaga, N., Nakao, T., Koyanagi, S., Ohdo, S., Yamaguchi, Y., Hamachi, I., Ono, M. & Ojida, A. Selective and reversible modification of kinase cysteines with chlorofluoroacetamides. *Nat. Chem. Biol.* **15**, 250–258 (2019).
19. Siemeister, G., Mengel, A., Fernández-Montalván, A. E., Bone, W., Schröder, J., Zitzmann-Kolbe, S., Briem, H., Prechtl, S., Holton, S. J., Mönning, U., von Ahsen, O., Johanssen, S., Cleve, A., Pütter, V., Hitchcock, M., von Nussbaum, F., Brands, M., Ziegelbauer, K. & Mumberg, D. Inhibition of BUB1 Kinase by BAY 1816032 Sensitizes Tumor Cells toward Taxanes, ATR, and PARP Inhibitors *In Vitro* and *In Vivo*. *Clin. Cancer Res.* **25**, 1404–1414 (2019).
20. Singh, J., Petter, R. C., Baillie, T. A. & Whitty, A. The resurgence of covalent drugs. *Nat. Rev. Drug Discov.* **10**, 307–317 (2011).

21. Kwak, E. L., Sordella, R., Bell, D. W., Godin-Heymann, N., Okimoto, R. A., Brannigan, B. W., Harris, P. L., Driscoll, D. R., Fidias, P., Lynch, T. J., Rabindran, S. K., McGinnis, J. P., Wissner, A., Sharma, S. V., Isselbacher, K. J., Settleman, J. & Haber, D. A. Irreversible inhibitors of the EGF receptor may circumvent acquired resistance to gefitinib. *Proc. Natl. Acad. Sci. U. S. A.* **102**, 7665 (2005).
22. Yun, C.-H., Mengwasser, K. E., Toms, A. V., Woo, M. S., Greulich, H., Wong, K.-K., Meyerson, M. & Eck, M. J. The T790M mutation in EGFR kinase causes drug resistance by increasing the affinity for ATP. *Proc. Natl. Acad. Sci.* **105**, 2070–2075 (2008).
23. Kawashima, S. A., Yamagishi, Y., Honda, T., Ishiguro, K. & Watanabe, Y. Phosphorylation of H2A by Bub1 Prevents Chromosomal Instability Through Localizing Shugoshin. *Science* **327**, 172–177 (2010).
24. McGuinness, B. E., Anger, M., Kouznetsova, A., Gil-Bernabé, A. M., Helmhart, W., Kudo, N. R., Wuensche, A., Taylor, S., Hoog, C., Novak, B. & Nasmyth, K. Regulation of APC/C Activity in Oocytes by a Bub1-Dependent Spindle Assembly Checkpoint. *Curr. Biol.* **19**, 369–380 (2009).
25. Perera, D. & Taylor, S. S. Sgo1 establishes the centromeric cohesion protection mechanism in G2 before subsequent Bub1-dependent recruitment in mitosis. *J. Cell Sci.* **123**, 653–659 (2010).
26. Klebig, C., Korinth, D. & Meraldi, P. Bub1 regulates chromosome segregation in a kinetochore-independent manner. *J. Cell Biol.* **185**, 841–858 (2009).
27. Ricke, R. M., Jeganathan, K. B., Malureanu, L., Harrison, A. M. & van Deursen, J. M. Bub1 kinase activity drives error correction and mitotic checkpoint control but not tumor suppression. *J. Cell Biol.* **199**, 931–949 (2012).
28. Scott, S. J., Suvarna, K. S. & D'Avino, P. P. Synchronization of human retinal pigment epithelial-1 cells in mitosis. *J. Cell Sci.* **133**, jcs247940 (2020).
29. Vassilev, L. T., Tovar, C., Chen, S., Knezevic, D., Zhao, X., Sun, H., Heimbrook, D. C. & Chen, L. Selective small-molecule inhibitor reveals critical mitotic functions of human CDK1. *Proc. Natl. Acad. Sci.* **103**, 10660–10665 (2006).
30. Mayer, T. U. Small Molecule Inhibitor of Mitotic Spindle Bipolarity Identified in a Phenotype-Based Screen. *Science* **286**, 971–974 (1999).
31. Brito, D. A. & Rieder, C. L. Mitotic Checkpoint Slippage in Humans Occurs via Cyclin B Destruction in the Presence of an Active Checkpoint. *Curr. Biol.* **16**, 1194–1200 (2006).
32. Goto, H., Yasui, Y., Nigg, E. A. & Inagaki, M. Aurora-B phosphorylates Histone H3 at serine28 with regard to the mitotic chromosome condensation: H3-Ser28 phosphorylation by Aurora-B. *Genes Cells* **7**, 11–17 (2002).
33. Ditchfield, C., Johnson, V. L., Tighe, A., Ellston, R., Haworth, C., Johnson, T., Mortlock, A., Keen, N. & Taylor, S. S. Aurora B couples chromosome alignment with anaphase by targeting BubR1, Mad2, and Cenp-E to kinetochores. *J. Cell Biol.* **161**, 267–280 (2003).
34. Zhao, Q., Ouyang, X., Wan, X., Gajiwala, K. S., Kath, J. C., Jones, L. H., Burlingame, A. L. & Taunton, J. Broad-Spectrum Kinase Profiling in Live Cells with Lysine-Targeted Sulfonyl Fluoride Probes. *J. Am. Chem. Soc.* **139**, 680–685 (2017).
35. Cravatt, B. F., Wright, A. T. & Kozarich, J. W. Activity-Based Protein Profiling: From Enzyme Chemistry to Proteomic Chemistry. *Annu. Rev. Biochem.* **77**, 383–414 (2008).
36. Schindelin, J., Arganda-Carreras, I., Frise, E., Kaynig, V., Longair, M., Pietzsch, T., Preibisch, S., Rueden, C., Saalfeld, S., Schmid, B., Tinevez, J.-Y., White, D. J., Hartenstein, V., Eliceiri, K., Tomancak, P. & Cardona, A. Fiji: an open-source platform for biological-image analysis. *Nat. Methods* **9**, 676–682 (2012).